average to the same value for the various sets of degenerate levels.

The emission spectrum at 45 K fits very nicely into this picture. The main sharp band, which coincides with the hot absorption band at 7586 cm^{-1}, is assigned to the transitions $|S_a = S = 0\text{–}15\rangle$ $(^1E_g) \rightarrow |S_a = S = 0\text{–}15\rangle$ $(^3A_{2g})$. In addition, the two broad wings on the low- and high-energy sides of this peak contain the overlapping transition to the other levels of the ground-state multiplet. The density of states for the ground-state manifold is plotted underneath the emission spectrum in Figure 4. The correlation with the experimental intensity distribution is excellent on the high-energy side of the $|S_a = S\rangle$ central peak. On the low-energy side the correlation is less perfect. In this spectral region there is a superposition of additional bands, which grow in intensity with decreasing temperature. These bands cannot be explained within the framework of the present model. They are most likely transitions to spin configurations different from the relaxed ground-state discussed in this paper, and these spin configurations may well originate from higher order lattice effects as T_N of $MnCl_2$ is reached. We are presently engaged in a more detailed study of these effects.

The effects observed here as well as the formalism used for their interpretation have a certain analogy to the magnon sidebands observed in the optical spectra of magnetically ordered compounds.[11] Positions and shapes of magnon sidebands are determined by the energy dispersion, i.e. the strength of the exchange coupling and the density of magnon states.

Finally we turn to a brief discussion of the weak sidebands observed below 10 K in the high-resolution absorption spectra (Figure 3). The most intense band at 7998 cm^{-1} (1.5 K), which is separated by 225 cm^{-1} from the main band, could be an a_{1g} vibrational sideband of the electronic origins. This is supported by the observed shift to lower energy between 10 and 30 K, which parallels the shift of the main band. The weak bands on the low-energy side of the main peak in the 1.5 K spectrum, which cannot be vibrational sidebands, are attributed to slightly perturbed Ti^{2+} centers. Nearest- and next-nearest-neighbor Ti^{2+} pairs, which are present in small concentrations in a crystal with 1% Ti^{2+}, are the most likely candidates.

(11) Sell, F. D.; Greene, R. L.; White, R. M. *Phys. Rev.* **1967**, *158*, 489.

6. Conclusions

The main near-infrared spectroscopic features of Ti^{2+} in $MnCl_2$ are explained remarkably well by using the one-parameter spin cluster model with $J = -6.2$ cm^{-1}. The fact the Ti^{2+}–Mn^{2+} interactions are 1–2 orders of magnitude larger than the Mn^{2+}–Mn^{2+} interactions is probably one of the main reasons for the success of the model. The model could thus potentially be applied to other systems of paramagnetic ions in paramagnetic host lattices, provided that the dopant–host interactions are the dominant ones. To the chemist, such a molecular approach to a solid-state problem is conceptually a very attractive one. The system of Ti^{2+} as an impurity in $MnCl_2$ offers advantages over other such magnetic host systems that have caught the attention of workers in this field, e.g. Ni^{2+} in MnI_2[6] and Cr^{3+} in $GdAlO_3$.[12–14] Since the formally spin-forbidden absorptions of Ti^{2+} have little or no single-ion intensity and are completely exchange-induced, there is no ambiguity as to which mechanism is the dominant one. Also the fact that Ti^{2+} has zero spin in the excited state greatly simplifies both the theoretical treatment and the experimental assignment of absorption bands. In addition, the system is well suited to luminescence studies, which provide an extra method of probing the ground-state properties.

Acknowledgment. We are grateful to the Royal Society for a fellowship under the European Science Exchange Programme (to S.M.J.).

(12) Helman, J. S.; Baltensperger, W. *Phys. Rev. B: Condens. Matter* **1982**, *25*, 6847.
(13) Aoyagi, K.; Kajiura, M.; Sugano, S. *J. Phys. Soc. Jpn.* **1981**, *50*, 3725.
(14) Kita, T.; Tanabe, Y. *J. Phys. Soc. Jpn.* **1985**, *54*, 2293.

Contribution from the Department of Chemistry,
Univeristy of Michigan, Ann Arbor, Michigan 48109

Relativistically Parametrized Extended Hückel Calculations. 11. Energy Bands for Elemental Tellurium and Polonium

Lawrence L. Lohr

Received October 9, 1986

An extension of the REX relativistically parametrized extended Hückel LCAO molecular orbital method to periodic solids is outlined. The method provides a simple and systematic approach to the description of the spin–orbit splitting of energy bands. The method is illustrated with results for the main-group elements tellurium and polonium, with trigonal-helical and simple-cubic structures, respectively. The helical structure of tellurium is described as a distortion of a simple-cubic structure, with the distortion being quenched in the case of polonium by its very large spin–orbit coupling.

Introduction

In 1979 we outlined[1] a relativistically parametrized version entitled REX of the extended Hückel molecular orbital method. The method differs from standard extended Hückel schemes[2,3] in that it employs an atomic $|lsjm\rangle$ complex spin–orbital basis rather than a real basis without spin. This complex basis, when combined with the standard Hückel assumption of effective Hamiltonian matrix elements being proportional to the corresponding overlap matrix elements, permits the systematic incorporation of spin–orbit coupling into the calculations. In addition the energy parametrization and choice of orbital exponents may be taken to reflect the other two important relativistic effects[4,5] in atomic structure, namely the contraction and stabilization of those orbitals of low total angular momentum, particularly $s_{1/2}$ and $p_{1/2}$ levels, and the self-consistent expansion and destabilization of those orbitals of high total angular momentum. The REX method[1,6] has been used in a number of studies[7–15] of the electronic

(1) Lohr, L. L.; Pyykkö, P. *Chem. Phys. Lett.* **1979**, *62*, 333.
(2) Hoffmann, R. *J. Chem. Phys.* **1963**, *39*, 1397.
(3) Howell, J.; Rossi, A.; Wallace, D.; Haraki, K.; Hoffmann, R. *QCPE* **1973**, *10* (Suppl.), 344.
(4) Pitzer, K. S. *Acc. Chem. Res.* **1979**, *12*, 271.
(5) Pyykkö, P.; Desclaux, J. P. *Acc. Chem. Res.* **1979**, *12*, 276.
(6) Lohr, L. L.; Hotokka, M.; Pyykkö, P. *QCPE* **1980**, *12*, 387.
(7) Lohr, L. L.; Hotokka, M.; Pyykkö, P. *Int. J. Quantum Chem.* **1980**, *18*, 34.
(8) Pyykkö, P.; Lohr, L. L. *Inorg. Chem.* **1981**, *20*, 1950.
(9) Pyykkö, P.; Wiesenfeld, L. *Mol. Phys.* **1981**, *43*, 557.

0020-1669/87/1326-2005$01.50/0

structure of compounds containing one or more elements of high atomic number; these include studies of actinide and lanthanide complexes,[8,13,15] main-group anionic clusters,[10] and nuclear spin–spin couplings.[9,11,12]

In the present study we outline an adaptation of the REX method to the description of materials with translational symmetry in one, two, or three dimensions, this adaptation thus permitting application of the REX method to polymers and solids with periodic boundary conditions. The resulting method, which we call REXBAND, is thus simply a relativistically parametrized variant of the tight-binding extended Hückel method[16-19] for periodic systems, the tight-binding method having been proven to be of considerable utility in understanding the electronic and geometrical structures of a wide variety of materials.

Method

The REXBAND method may be easily described, as it is simply an extension of the REX method with its $|lsjm\rangle$ complex spin–orbital basis to periodic systems via the introduction of Bloch functions $\phi_\alpha(\mathbf{r},\mathbf{k})$, where

$$\phi_\alpha(\mathbf{r},\mathbf{k}) = \sum e^{i\mathbf{k}\cdot\mathbf{R}_{\alpha j}} f(\mathbf{r} - \mathbf{R}_{\alpha j}) \qquad (1)$$

in which α denotes an orbital type, $\mathbf{k}$ is the wave vector, $\mathbf{R}_{\alpha j}$ is the position in cell j of the atom with orbital f_α of type α, and the summation is over cells.

The actual molecular orbitals (MO's) for the periodic system are given by solution of the generalized secular equation

$$\mathbf{H}(\mathbf{k})\,\mathbf{C}(\mathbf{k}) = \mathbf{S}(\mathbf{k})\,\mathbf{C}(\mathbf{k})\,\lambda^{\mathrm{D}}(\mathbf{k}) \qquad (2)$$

where $\mathbf{C}(\mathbf{k})$ is the matrix whose columns are the complex eigenvectors, $\lambda^{\mathrm{D}}(\mathbf{k})$ is the real diagonal matrix whose nonzero elements are the eigenvalues, $\mathbf{S}(\mathbf{k})$ is the $n \times n$ overlap matrix given by

$$\mathbf{S}(\mathbf{k}) = \sum e^{i\mathbf{k}\cdot\mathbf{R}_j}\mathbf{S}^j \qquad (3)$$

in which $\mathbf{S}^j$ is the $n \times n$ overlap matrix between the n functions in the reference cell ($j = 0$) and the translationally related n functions in the jth cell, $\mathbf{R}_j$ is the vector location of the jth cell, and $\mathbf{H}(\mathbf{k})$ is the effective one-electron Hamiltonian matrix similarly constructed as

$$\mathbf{H}(\mathbf{k}) = \sum e^{i\mathbf{k}\cdot\mathbf{R}_j}\mathbf{H}^j \qquad (4)$$

The standard extended Hückel assumptions are used to construct $\mathbf{H}^\circ$ (interactions within the reference cell), namely that the diagonal elements $H^\circ_{\alpha\alpha}$ are input parameters and that the off-diagonal elements $H^\circ_{\alpha\beta}$ are related to the corresponding overlap matrix elements via

$$H^\circ_{\alpha\beta} = (1.75/2)(H^\circ_{\alpha\alpha} + H^\circ_{\beta\beta})S^\circ_{\alpha\beta} \qquad \alpha \neq \beta \qquad (5)$$

The diagonal and off-diagonal elements of $\mathbf{H}^j$ ($j \neq 0$) then become

$$H^j_{\alpha\alpha} = (1.75/2)H_{\alpha\alpha}S^j_{\alpha\alpha} \qquad (6a)$$

$$H^j_{\alpha\beta} = (1.75/2)(H^\circ_{\alpha\alpha} + H^\circ_{\beta\beta})S^j_{\alpha\beta} \qquad \alpha \neq \beta \qquad (6b)$$

such that $H_{\alpha\alpha}(\mathbf{k})$ is related to $S_{\alpha\alpha}(\mathbf{k})$ via

$$H_{\alpha\alpha}(\mathbf{k}) = H^\circ_{\alpha\alpha}[1 + 1.75(S_{\alpha\alpha}(\mathbf{k}) - 1)] \qquad (7)$$

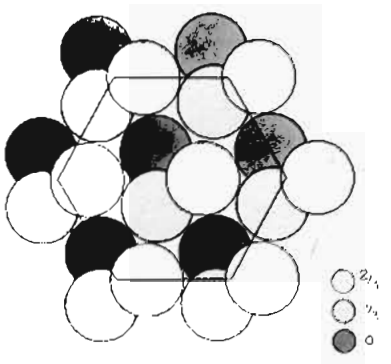

Figure 1. View along the c axis of the tellurium structure, D_3^4 ($P3_121$). Atoms are located at $(-u, -u, 0)$, $(u, 0, {}^1/_3)$, and $(0, u, {}^2/_3)$, with $u = 0.2633$.

while the relationship of $H_{\alpha\beta}(\mathbf{k})$ to $S_{\alpha\beta}(\mathbf{k})$ for $\alpha \neq \beta$ parallels the relationship in (5) or (6b).

As previously outlined by us,[1] the overlap matrix in the $|lsjm\rangle$ basis is central to the REX method and is calculated by supplying as input data *two* sets of real atomic orbitals for each atom. The first and second sets consist of those orbitals whose radial functions are later associated with the $j = l - {}^1/_2$ and $j = l + {}^1/_2$ orbitals, respectively. The standard routines for calculating the real overlap matrix in the real atomic orbital (AO) basis are employed. A unitary transformation is then used to construct the overlap matrix in the desired basis. For example, the three real p AO's of the first set are used to construct the two functions $j = {}^1/_2$, $m = \pm{}^1/_2$, while the second set of three real p AO's are used to construct the four functions $j = {}^3/_2$, $m = \pm{}^3/_2, \pm{}^1/_2$. This is carried out separately for each atom-pair block of the original real overlap matrix and separately for α and β spins. In the new REXBAND procedure this transformation follows the construction of $\mathbf{S}(\mathbf{k})$ according to (3); that is, the complex $\mathbf{S}(\mathbf{k})$ is obtained via (3) from a set of real $\mathbf{S}^j$ for a suitably chosen range of cells neighboring the reference cell, and then the REX transformation to $\mathbf{S}(\mathbf{k})$ in the $|lsjm\rangle$ basis is made. The construction in REXBAND of $\mathbf{H}(\mathbf{k})$ is then made directly in the $|lsjm\rangle$ basis using (4)–(6). Minor computational details are skipped here, but it should be noted that population analysis routines must be modified to take into account that the diagonal elements of $\mathbf{S}(\mathbf{k})$ are in general not equal to unity.

Applications: Tellurium and Polonium

To illustrate the usefulness of the REXBAND procedure, we consider the electronic structures of the solid elements tellurium and polonium and seek to answer the following question: Why is tellurium helical, while polonium is simple cubic?

Tellurium, like the so-called "metallic" form of selenium, possesses a structure[20] having the chiral trigonal space group D_3^4 ($P3_121$) or D_3^6 ($P3_221$). In a hexagonal description there are three atoms per unit cell at the positions $(-u, -u, 0)$, $(u, 0, {}^1/_3)$, and $(0, u, {}^2/_3)$ with parameters $a = 4.4572$ Å, $c = 5.929$ Å, and $u = 0.2633$. Each Te has two neighbors (cis) at 2.835 ± 0.002 Å with an angle of $103.2 \pm 0.1°$ between these bonds and four neighbors at 3.495 ± 0.003 Å; the next nearest neighbors along the chain are at 4.445 ± 0.001 Å. Figure 1 shows this structure as viewed along the c axis. As discussed later and pointed out by von Hippel,[21] this structure may be viewed as a helical distortion from a simple-cubic structure. The latter obtains for the special case of $c/a = ({}^3/_2)^{1/2} = 1.22474$ and $u = {}^1/_3$; for Te c/a is larger than this, namely 1.3302, while u is smaller, namely 0.2633, as noted.

Polonium exhibits two structural forms:[22a] the better known α phase with its simple cubic O_h^1 ($Pm3M$) structure, $a = 3.345 \pm 0.002$ Å, and the β phase, stable[22b] above 77 ± 9 °C, with its rhombohedral D_{3d}^5 ($R3m$) structure, $a = 3.359 \pm 0.002$ Å, $\alpha = 98.22 \pm 0.05°$. For each the coordination number is 6. One of

(10) Lohr, L. L. *Inorg. Chem.* **1981**, *20*, 4229.
(11) Pyykkö, P. *J. Organomet. Chem.* **1982**, *232*, 21.
(12) Viste, A.; Hotokka, M.; Laaksonen, L.; Pyykkö, P. *Chem. Phys.* **1982**, *72*, 225.
(13) Pyykkö, P.; Laaksonen, L. *J. Phys. Chem.* **1984**, *88*, 4892.
(14) Larsson, S.; Pyykkö, P. *Chem. Phys.* **1986**, *101*, 355.
(15) Lohr, L. L.; Jia, Y. Q. *Inorg. Chim. Acta* **1986**, *119*, 99.
(16) Burdett, J. K. *Prog. Solid State Chem.* **1984**, *15*, 17.
(17) Albright, T. A.; Burdett, J. K.; Whangbo, M.-H. *Orbital Interactions in Chemistry*; Wiley: New York, 1985.
(18) Whangbo, M.-H.; Schneemeyer, L. F. *Inorg. Chem.* **1986**, *25*, 2424.
(19) Whangbo, M.-H.; Brec, R.; Ouvrad, G.; Rouxel, J. *Inorg. Chem.* **1985**, *24*, 2459.
(20) Cherin, P.; Unger, P. *Acta Crystallogr.* **1967**, *23*, 670.
(21) von Hippel, A. *J. Chem. Phys.* **1948**, *16*, 372.
(22) (a) Beamer, W. H.; Maxwell, C. R. *J. Chem. Phys.* **1949**, *17*, 1293. (b) Maxwell, C. R. *J. Chem. Phys.* **1949**, *17*, 1288.

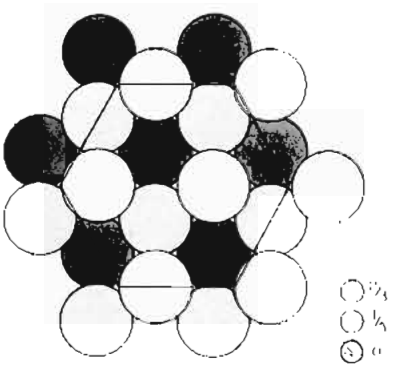

Figure 2. View along the C_3 axis of the polonium structure, O_h^1 ($Pm3m$). Atoms are located at $(-u, -u, 0)$, $(u, 0, {}^1/_2)$, and $(0, u, {}^2/_3)$, with $u = {}^1/_3$.

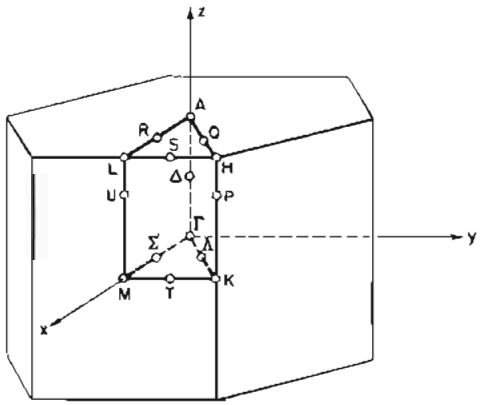

Figure 3. Brillouin zone for the hexagonal Bravais lattice. See ref 24 and 25 for definitions of the special lines and points.

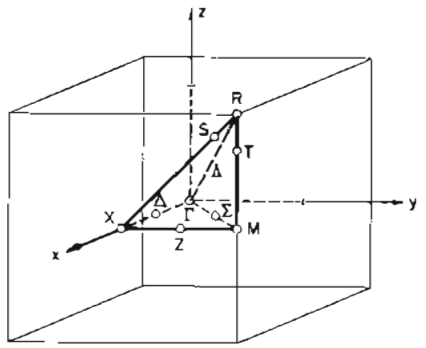

Figure 4. Brillouin zone for the simple-cubic Bravais lattice. See ref 24 and 35 for definitions of the special lines and points.

the two high-pressure forms[23] of Te also is rhombohedral, namely that stable above 70 kbar with $a = 3.002 \pm 0.015$ Å and $\alpha = 103.3 \pm 3.0°$ (data at 115 kbar). The other phase (40–70 kbar) is of uncertain structure. Figure 2 shows the simple cubic structure of Po in a trigonal view to match the orientation of Figure 1.

Figures 3 and 4 show the Brillouin zones for hexagonal and simple-cubic Bravais lattices, these corresponding to the Te and Po structures, respectively. Conventional notation[24] is employed for the special directions and points in k space. Figure 5 shows the 5p valence and conduction bands of Te for most of these special directions and points as obtained with the relativistic parameters in Table I. Individual bands are not shown, only the envelopes for the valence and conduction bands. The highest occupied level is that at **H** where $\mathbf{k} = ({}^1/_3, {}^1/_3, {}^1/_2)$; the vertical gap is 2.5 eV, while the indirect gap to a point near A [near $\mathbf{k} = (0, 0, {}^1/_2)$] is 1.1 eV. This calculated gap is too large; various measurements[25-27]

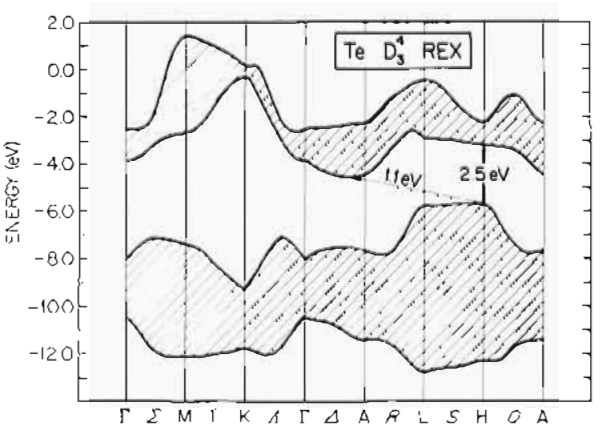

Figure 5. Envelopes of the Te 5p valence (lower) and conduction (upper) bands as obtained with the relativistic parameters from Table I. Calculations were made at the symmetry points (vertical lines) and at four points between each pair of symmetry points.

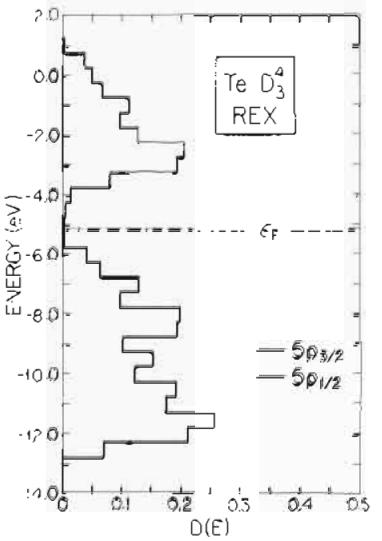

Figure 6. Density of states for Te 5p bands as obtained from energies at 100 randomly selected points in k space.

Table I. REXBAND Parameters

		Te		Po	
		EHT	REX	EHT	REX
α^a	ns	−19.12	−20.39	−17.96	−22.04
α	$np_{1/2}$	−9.54	−10.10	−9.05	−10.98
α	$np_{3/2}$	−9.54	−9.22	−9.05	−8.22
ζ^b	ns	2.470	2.568	2.720	3.067
ζ	$np_{1/2}$	2.036	2.117	2.245	2.538
ζ	$np_{3/2}$	2.036	2.025	2.245	2.211

[a] Energy parameters in eV. [b] Slater exponents in au^{-1}.

have indicated a band edge of 0.335 eV. While we certainly could carry out variations of the input parameters or expansion of the basis set to obtain a smaller gap, we have not done so, as reproduction of the observed gap was not our objective. Indeed there have been a number of energy band calculations before for tellurium and the isostructural selenium.[28-34]

(23) Jamieson, J. C.; McWhan, D. M. *J. Chem. Phys.* **1965**, *43*, 1149.
(24) Slater, J. C. *Quantum Theory of Molecules and Solids*; McGraw-Hill: New York, 1965; Vol. 2.
(25) Tutihasi, S.; Roberts, G. G.; Keezer, R. C.; Drews, R. E. *Phys. Rev.* **1969**, *177*, 1143.
(26) Stolze, H.; Lutz, M.; Grosse, P. *Phys. Status Solidi B* **1977**, *82*, 457.
(27) Anzin, V. B.; Eremets, M. I.; Kosichkin, Yu. V.; Nadezhdinskii, A. I.; Shirokov, A. M. *Phys. Status Solidi A* **1977**, *42*, 385.
(28) Gaspar, R. *Acta Phys. Acad. Sci. Hung.* **1957**, *7*, 289.
(29) Reitz, J. R. *Phys. Rev.* **1957**, *105*, 1233.
(30) de Carvalho, A. P. *C. R. Hebd. Seances Acad. Sci.* **1959**, *248*, 778.
(31) Beissner, R. E. *Phys. Rev.* **1966**, *145*, 479.

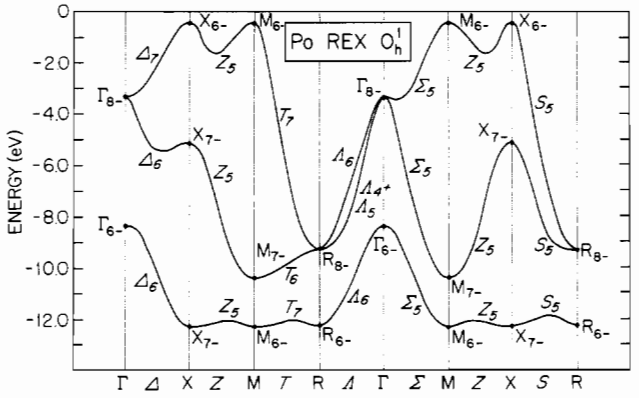

Figure 7. Energies of the Po 6p bands as obtained with the relativistic parameters from Table I. Calculations were made at the symmetry points (vertical lines) and at four points between each pair of symmetry points.

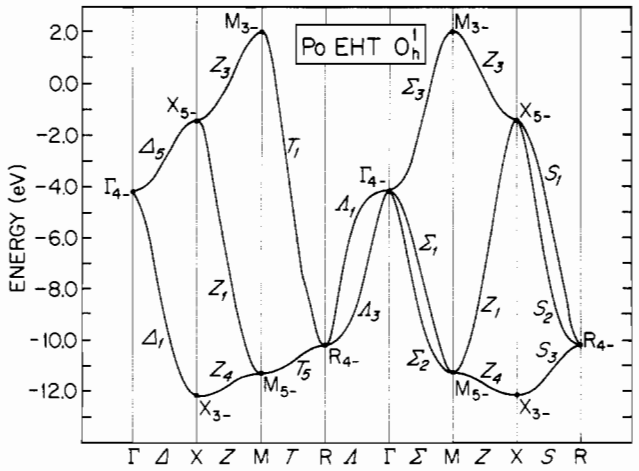

Figure 8. Energies of the Po 6p bands based on the nonrelativistic parameter from Table I. Calculations were made at symmetry points and at four points between each pair of symmetry points.

Figure 6 shows the density of states (DOS) for Te constructed as a histogram from REX calculations carried out at 100 randomly selected points (no symmetry points except by chance) in **k** space. The resulting energy eigenvalues were assigned to 0.5 eV wide bins. Also shown in Figure 6 is the input atomic spin–orbit splitting from Table I, this splitting being very small compared to the dispersion. Two-thirds of the p-band DOS falls below the Fermi level (E_F); one-third, above. The tendency to form a separate $5p_{1/2}$ band is minimal.

We next present in more detail the principal ojbect of our study, namely the band structures of Po. Figures 7 and 8 show the REX and EHT band structures based respectively upon the relativistic and nonrelativistic parameters from Table I, while Figures 9 and 10 show the corresponding REX and EHT DOS plots, each of the latter based upon calculations at 200 randomly selected points in **k** space. We note that by symmetry it is irrelevant whether or not the selection is restricted to the asymmetric unit (the "irreducible wedge") of the Brillouin zone. Individual bands (omitting the predominantly 6s band) are shown in Figures 7 and 8, with conventional labels for the states according to the irreducible representations[35] of the translational group with and without electron spin, respectively, the connections across the symmetry points illustrating the well-known compatibility relations for O_h.[1] The input atomic spin–orbit splitting is large, namely

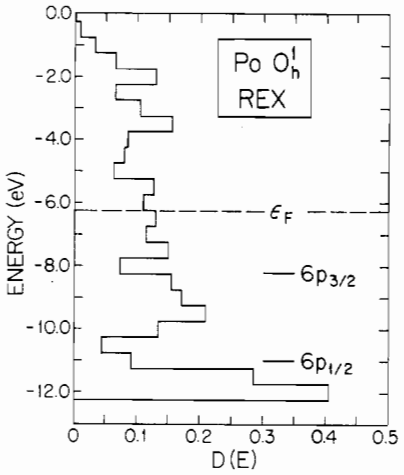

Figure 9. Density of states for Po 6p bands as obtained from relativistic energies at 200 randomly selected points in **k** space.

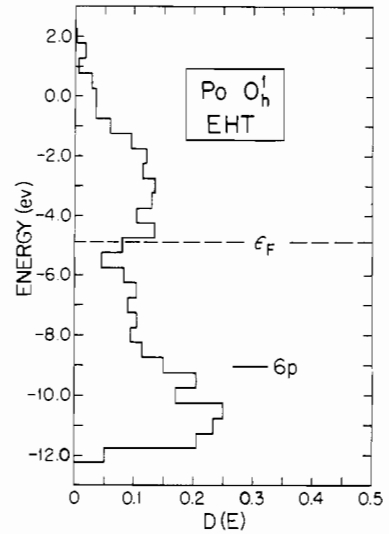

Figure 10. Density of states for Po 6p bands based on nonrelativistic energies at 200 randomly selected points in **k** space.

2.76 eV (Table I and Figure 9), and the $6p_{1/2}$ function is more contracted than the $6p_{3/2}$, with ζ values of 2.538 and 2.211, respectively (Table I). These and other parameters are simply the REX default values, with ζ's taken from Desclaux' numerical Dirac–Fock (DF) and Hartree–Fock (HF) atomic eigenvalues[36] and with ζ related to Desclaux' electron mean radii $\bar{r}$ by $\zeta = (n + {}^1/_2)/\bar{r}$, where n is the principal quantum number. We note in Figure 9 the strong tendency toward formation of a separate $6p_{1/2}$ band, leaving the $6p_{3/2}$ band half-filled and making simple-cubic Po metallic. Thus, we suggest that it is the very large spin–orbit coupling in Po that stabilizes the simple-cubic metallic structure by suppressing the group VIA (group 16) tendency to form two strong covalent bonds approximately 90° apart, as the latter would require "free" use of the appropriate p functions. Recall that each $p_{1/2}$ function has a spherical charge distribution corresponding to a density arising from one-third each of p_x, p_y, and p_z. Withdrawal of $p_{1/2}$ from chemical bonding leaves $p_{3/2}$, from which strongly localized bonds cannot be formed.

We are not in a position to comment on the stability of α-Po (simple cubic) relative to β-Po (simple rhombohedral); both, as noted, have a coordination number of 6. The relationship of the α-Po structure to the NaCl-type Pb chalcogenide structures has been noted in X-ray studies of Pb–Po solid solutions, with the simple-cubic α-Po structure obtaining in the limit of zero Pb content.

(32) Treusch, J. O.; Sandrock, R. *Phys. Status Solidi* **1966**, *16*, 487.
(33) Kramer, B.; Thomas, P. *Phys. Status Solidi* **1968**, *26*, 151.
(34) Hulin, M.; Picard, M. *Solid State Commun.* **1969**, *7*, 1587.
(35) Miller, S. C.; Love, W. F. *Tables of Irreducible Representations of Space Groups and Co-representations of Magnetic Space Groups*; Pruett: Boulder, CO, 1967.
(36) Desclaux, J. P. *At. Data Nucl. Data Tables* **1973**, *12*, 311.

Summary

We have outlined an extension of the REX semiempirical molecular orbital method to periodic systems. The method provides a simple and systematic approach to the description of the spin–orbit splitting of energy bands. The method is illustrated with results for tellurium and polonium, with trigonal-helical and simple-cubic structures, respectively; the helical structure of tellurium is described as a distortion of a simple-cubic structure, with the distortion being quenched in the case of polonium by its very large spin–orbit coupling.

Acknowledgment. I thank Y. Q. Jia of the People's Republic of China for his assistance with this project and Professor J. K. Burdett of the University of Chicago for very helpful suggestions. I also thank the University of Michigan Computing Center for the use of its facilities.

Notes

Contribution from the Inorganic Chemistry Laboratory, University of Oxford, Oxford OX1 3QR, England

High-Yield One-Step Synthesis of 1,4,7-Trithiacyclononane (9S3)

Philip J. Blower and Stephen R. Cooper*

Received February 3, 1987

In 1983 Glass and co-workers reported the first complex of 1,4,7-trithiacyclononane (9S3),[1] a ligand originally synthesized

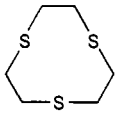

9S3

by Ochrymowycz et al. in 1974.[2,3] Intensive work by a number of groups has subsequently shown that 9S3 forms complexes with a wide variety of transition-metal ions.[1,4-11] These complexes are remarkably robust, presumably because the nine-membered ring constrains the S atoms to virtually the same positions in the free ligand[12] as in its complexes.[1,4-11] Moreover, they often have exceptional redox and electronic properties. For example, $[Rh(9S3)_2]^{3+}$ readily undergoes two successive one-electron reductions to yield $[Rh(9S3)_2]^{+}$ via a rare example of a stable monomeric Rh(II) complex.[10] Both the investigation of the reactivity of these unusual complexes and the obvious utility of 9S3 as a capping ligand ensure that work on this macrocycle will continue to expand at its present impressive pace.

A major impediment to work on this ligand, however, has been its preparation. Owing to the difficulty of closing a nine-membered ring, synthesis of 9S3 has been a thorny problem. The original synthesis gave 9S3 in only 0.04% yield,[2] which subsequent work raised first to 4.4%[1] and then to 20%[6]. These procedures are not suited to scaling up to multigram quantities because they require separation of 9S3 from its higher homologues and polymers by column chromatography. Recently Sellmann and Zapf[13] published an ingenious $Mo(CO)_3$-mediated cyclization of 2-mercaptoethyl sulfide that gives 9S3 in high yield. Because this route involves several steps and a considerable amount of manipulation, it is inconvenient for large-scale preparation of the ligand. We report here a high-yield (50%) route that proceeds in one step from commercially available materials and can be used to prepare pure 9S3 in large quantities without column chromatography.

Experimental Section

All reagents were supplied by Aldrich Chemical Co. Ltd. and used as received, except 2-mercaptoethyl sulfide, which was vacuum distilled prior to use.

1,4,7-Trithiacyclononane (9S3). Finely powdered anhydrous cesium carbonate (13.03 g, 40 mmol) was suspended in *N,N*-dimethylformamide (DMF) (250 mL, from a freshly opened bottle) under a dinitrogen atmosphere. To the vigorously stirred suspension maintained at 100 °C was added a solution of 2-mercaptoethyl sulfide (5.56 g, 36 mmol) and 1,2-dichloroethane (3.54 g, 36 mmol) in DMF (150 mL) from a dropping funnel at a rate of 5 mL/h. After the addition was complete, stirring was continued at 100 °C for a further 12 h, after which the solvent was removed in vacuo. The residual white solid was extracted with CH_2Cl_2 (3 × 100 mL), and the filtered extract washed with 1.0 M aqueous NaOH (2 × 100 mL) and evaporated to dryness. The resulting sticky solid was washed with water (3 × 50 mL) and dissolved in CH_2Cl_2 (100 mL). The solution was dried over $MgSO_4$ and evaporated to dryness. The residue was placed in a sublimation apparatus and heated at 90 °C under vacuum, whereupon the product crystallized as a white solid on the water-cooled cold finger (3.25 g, 50%); mp 79–80 °C. Anal. (Oxford Microanalytical Service) Calcd for $C_6H_{12}S_3$: C, 40.0; H, 6.7. Found: C, 40.0; H, 6.9. IR (Nujol mull, cm^{-1}): 2804 w, 1421 m, 1414 m, 1409 m, 1298 m, 1283 s, 1192 w, 1185 w, 1137 w, 1129 w, 987 w, 924 m, 879 s, 840 m, 825 s, 722 w, 671 m, 620 m. ^1H NMR ($CDCl_3$, δ, vs. Me_4Si) 3.13 s. The yield depends critically upon the rate of addition, with faster rates giving yields of approximately 35%. The ligand is soluble in dichloromethane, toluene, and diethyl ether, sparingly soluble in pentane and methanol, and insoluble in water.

Discussion

The major advantages of this procedure are the simplicity of the synthesis and the ease of the workup. All of the starting materials are commercially available, and isolation of the product by condensation from the vapor avoids recourse to column chromatography. Together these two features (especially the latter) permit ready scaling up of the procedure, so that large quantities of 9S3 can be made easily.

The synthesis makes use of the cesium carbonate mediated cyclization introduced by Kellogg and co-workers.[14,15] While there has been speculation on why Cs_2CO_3 favors cyclization over polymer formation,[15,16] its efficacy probably results from weak ion pairing between Cs^+ and RS^-, which generates an exceptionally nucleophilic thiolate anion. Under high dilution conditions the enhanced nucleophilicity of RS^- would particularly favor intra-

(1) Setzer, W. N.; Ogle, C. A.; Wilson, G. S.; Glass, R. S. *Inorg. Chem.* **1983**, *22*, 266–271.
(2) Ochrymowycz, L. A.; Gerber, D.; Chongsawangvirod, P.; Leung, A. K. *J. Org. Chem.* **1977**, *42*, 2644–5.
(3) 9S3 was first reported by Ray in 1920 (Ray, P. C. *J. Chem. Soc.* **1920**, 1090–2), but subsequent work[2] makes it clear that the isolated compound was in fact *p*-dithiane, not 1,4,7-trithiacyclonane.
(4) Ashby, M. T.; Lichtenberger, D. L. *Inorg. Chem.* **1985**, *24*, 636–8.
(5) Küppers, H.-J.; Wieghardt, K.; Weiss, J. *Inorg. Chem.* **1985**, *24*, 3067–71.
(6) Hartman, J. R.; Cooper, S. R. *J. Am. Chem. Soc.* **1986**, *108*, 1202–8.
(7) Küppers, H.-J.; Neves, A.; Pomp, C.; Ventur, D.; Wieghardt, K.; Nuber, B.; Weiss, J. *Inorg. Chem.* **1986**, *25*, 2400–8.
(8) Wilson, G. S.; Swanson, D. D.; Glass, R. S. *Inorg. Chem.* **1986**, *25*, 3827–9.
(9) Rawle, S. C.; Cooper, S. R. *J. Chem. Soc., Chem. Commun.* **1987**, 308–9.
(10) Rawle, S. C.; Yagbasan, R.; Prout, K.; Cooper, S. R. *J. Am. Chem. Soc.*, in press.
(11) Clarkson, J.; Yagbasan, R.; Blower, P. J.; Rawle, S. C.; Cooper, S. R. *J. Chem. Soc., Chem. Commun.*, in press.
(12) Glass, R. S.; Wilson, G. S.; Setzer, W. N. *J. Am. Chem. Soc.* **1980**, *102*, 5068–9.
(13) Sellmann, D.; Zapf, L. *Angew. Chem., Int. Ed. Engl.* **1984**, *23*, 807–8.
(14) Buter, J.; Kellogg, R. M. *J. Chem. Soc., Chem. Commun.* **1980**, 466–7.
(15) Buter, J.; Kellogg, R. M. *J. Org. Chem.* **1981**, *46*, 4481–5.
(16) Kruizinga, W. H.; Kellogg, R. M. *J. Am. Chem. Soc.* **1981**, *103*, 5183–9.

0020-1669/87/1326-2009$01.50/0